Particles II

Access the latest eBook →

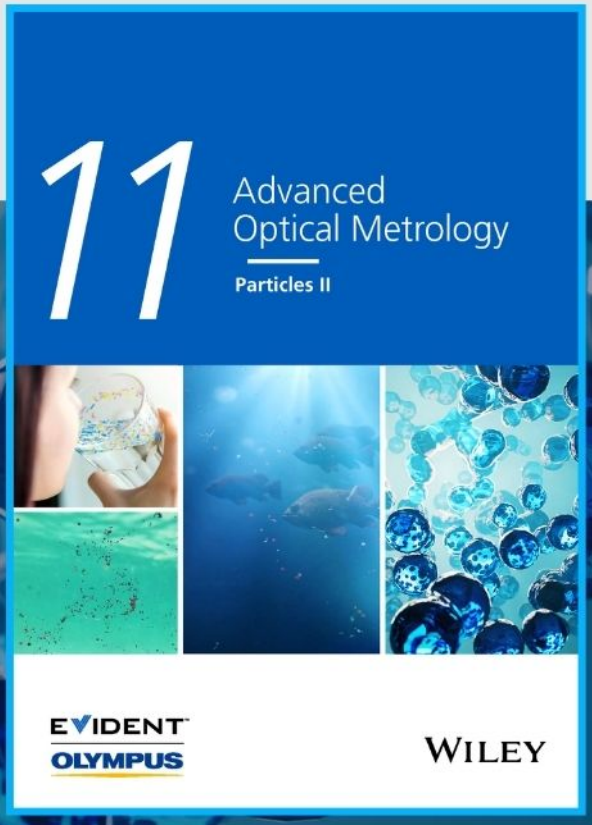

Impact on Biological Systems and the Environment

This eBook is dedicated to the research of Professor David Wertheim.
In collaboration with various groups, Professor Wertheim uses confocal microscopy to analyse the impact of different types of particles on human health and the environment, with a focus on human health-hazardous particles detected with solid-state nuclear track detectors (SSNTD). Download for free, today.

EVIDENT
OLYMPUS

WILEY

ADVANCED MATERIALS
www.advmat.de

Fabrication of Stretchable Superamphiphobic Surfaces with Deformation-Induced Rearrangeable Structures

Xiaoteng Zhou, Jie Liu, Wendong Liu, Werner Steffen, and Hans-Jürgen Butt*

Stretchable superamphiphobic surfaces with a high deformation resistance are in demand to achieve liquid-repellent performance in flexible electronics, artificial skin, and textile dressings. However, it is challenging to make mechanically robust superamphiphobic coatings, which maintain their superliquid repellency in a highly stretched state. Here, a stretchable superamphiphobic surface is reported, on which the microstructures can rearrange during stretching to maintain a stable superamphiphobicity even under a high tensile strain. The surface is prepared by spray-coating silicone nanofilaments onto a prestretched substrate (e.g., *cis*-1,4-polyisoprene) with poly(dimethylsiloxane) (PDMS) layer as a binder. After subsequent fluorination, this surface keeps its superamphiphobicity to both water and n-hexadecane up to the tensile strain of at least 225%. The binding PDMS layer and rearrangeable structures maximize the deformation resistance of the surface during the stretching process. The superamphiphobicity and morphology of the surface are maintained even after 1000 stretch–release cycles. Taking advantage of the mentioned benefits, a liquid manipulation system is designed, which has the potential for fabricating reusable and low-cost platforms for biochemical detection and lab-on-a-chip systems.

1. Introduction

Liquid-repellent surfaces are of interest for basic research and industrial use in self-cleaning,[1] antifouling,[2] corrosion resistance,[3] and droplet manipulation.[4] To achieve superliquid-repellency, the liquid needs to be in the Cassie state, in which a layer of air is entrapped between the liquid and the substrate.[5] For liquids with low surface tension (γ), the Cassie state with a static contact angle larger than 150° can be achieved on superamphiphobic surfaces with microscopic overhanging morphologies, sometimes called a re-entrant geometry.[6] Surfaces such as silicone nanofilaments[6c] or template candle soot[6d] have been reported to achieve superamphiphobicity by having a sub-micrometer inward curved surface morphology. Although we now profit from an improved understanding of the mechanisms of a superamphiphobic surface, a less complex method of preparation and a high mechanical stability of the surface are still two of the main challenges that have hindered its widespread adoption.[7]

Recently, superliquid-repellent surfaces with deformation-resistant performance are becoming increasingly significant in various situations such as flexible electronics,[8] artificial skin,[9] textile dressings,[10] and liquid manipulation.[11] Currently existing superamphiphobic surfaces appear to lose their superliquid-repellency to nonpolar liquids under small deformation, in particular when being stretched.[12] The breakup of the surface structures during stretching usually cause the low-surface-tension liquids on the surface transiting from the Cassie state to the Wenzel state (fully wetted) easily. Pan et al. reported an excellent textile which repels the wetting of liquid nitrogen with surface tension of 8.8 mN m^{-1}, yet it loses the superoleophobicity when being stretched to 20%.[12a] Even till now, there is no effective way proposed to solve this problem that the loss of superamphiphobicity due to stretching.

In this work, we fabricated a stretchable surface whose superamphiphobicity is maintained during stretching via construction of spontaneously rearrangeable microstructures, and which is fabricated by spray-coating silicone nanofilament (NF) on a pre-stretched elastic substrate. A single NF usually has a diameter of the order of 10 nm and can form on the overhanging structures due to its round, spaghetti-like shape.[6c] After spray-coating process, the NFs together with their assembly lead to a re-entrant geometry from tens of nanometer to hundreds of micrometers providing the underlying structure for a superamphiphobic surface. Releasing the tension of the substrate after fabrication leads to relatively compacted structures. During the surface stretching process, we observed the rearrangement of these structures in situ. The rearrangement of the structures includes the breakup of the largest NF clusters and the movement of the structures with respect to each other due to surface stretching. Through monitoring the size and density of the structure, the reason why the surface remains its superamphiphobicity in a high strain was understood.

X. Zhou, J. Liu
Key Laboratory of Green Printing, Institute of Chemistry
Chinese Academy of Sciences
Beijing 100190, China
X. Zhou, J. Liu, W. Liu, W. Steffen, H.-J. Butt
Max Planck Institute for Polymer Research
Ackermannweg 10, 55128 Mainz, Germany
E-mail: liujie@mpip-mainz.mpg.de
The ORCID identification number(s) for the author(s) of this article can be found under https://doi.org/10.1002/adma.202107901.

DOI: 10.1002/adma.202107901

This surface was further utilized to fabricate a programmable liquid manipulation system to achieve drop coalescences and synthesis of asymmetric hydrogels.

2. Results and Discussion

Spray-coating is a simple and effective method to construct hierarchical micro/nanostructures, but using nanoparticles in spray-coating to prepare superamphiphobic surfaces is usually a complex process. Particles size, concentration, spray pressure, droplet size, and solvent all need to be optimized in order to obtain a re-entrant structure.[10a,13] Silicone nanofilaments (NF) synthesized by cross-linking of hydrolyzed trichloromethylsilane (TCMS)[14] can easily form sub-microscale re-entrant structures, which are one of the most effective superamphiphobic coatings with ultralow sliding angles of liquids.[6c,15] However, direct growth of NF on the surface usually needs to be carried out under specific conditions including rinsing the surface in organic solvent or in vacuum. This significantly reduces the area that can be covered and the efficiency to modify the surface, thus limiting its widespread use.

To overcome the limits of NF direct growth and to reduce the complexity of the preparation, we use pre-prepared nanofilaments as the substitute of nanoparticles in spray-coating. Only a low spray pressure (27 kPa) is applied, as compared to the high spray pressure (150–300 kPa) that is normally used,[8b,16] which further facilitates the process. A poly(dimethylsiloxane) (PDMS, Sylgard184) layer is used as the binder to fix the NF layer on the substrate.[17] To achieve stretching stability of the superamphiphobicity, the pre-stretching of the substrate was carried out to ensure the surface to be covered by NF with a high density after spray-coating. The "pre-stretching" method of preparing stretching resistant superliquid-repellent surfaces was first proposed by Genzer et al.,[18] based on which various kinds of surfaces such as tunable surface patterns,[19] stretchable superhydrophobic surface,[20] hierarchically wrinkled surface[21] were developed. As a model substrate, a commercial *cis*-1,4-polyisoprene tape (Figure S1a,b, Supporting Information) was elongated to the tensile strain ε ($\varepsilon = (L - L_0)/L_0 \times 100\%$, in which L_0 is the original length of the relaxed surface and L is the stretched length) of 200% (**Figure 1**a). The solution of PDMS oligomers and curing agent (10:1) in n-hexane (4.2 wt%) was spray-coated on the stretched substrate (Figure S1c,d, Supporting Information). The thickness of the PDMS layer was 0.85 ± 0.10 μm (Figure S2, Supporting Information). Then the NF dispersion (0.1 wt% in toluene) was spray-coated onto the PDMS layer immediately. After curing at 80 °C for 2 h, the sample was fluorinated with trichloro(1H,1H,2H,2H-heptadecafluorodecylsilane) by chemical vapor deposition after activating the surface with oxygen plasma. The surface was always held in tension during the preparation. A permanent strain of 10.5% remained when releasing the surface to the relaxed state after pre-stretching to 200% (Figure S3, Supporting Information). We define the tensile strain of the relaxed surface after this permanent deformation as $\varepsilon_0 = 0\%$ for following tests. The permanent strain of the surface depends on the selected substrate, and might be improved by optimizing materials or preparation techniques.[22]

The nanofilament-structured and stretchable superamphiphobic (NFSS) surface shows a hierarchical micro/nanostructure (Figure 1b,c). To clearly present the morphology and the composition of the surface, we further observed the cross-section of the NFSS surface by SEM (Figure S4, Supporting Information). Comparing to the porous nanofilament structure on the top of the NF clusters, we observed a different morphology at a certain region close to the substrate. The nanofilament structure in this region is denser than that in the upper side. This dense layer is the binding layer composed of both nanofilament and cross-linked PDMS. The thickness is around 1.5 ± 0.5μm, which is much lower than the thickness (45 ± 20 μm) of the nanofilament layer. For the gaps existing on the substrate, the NF structure can only partially cover them. As the gaps are so small that extra nanofilaments cannot fill in them (Figure S5, Supporting Information).

As the NFSS surface is fabricated by keeping the substrate under tension, the NF microstructures become more compacted after the surface is released (Figure 1d). Thereby the NFSS surface at the relaxed state exhibits both advancing (Θ_{ACA}) and receding (Θ_{RCA}) contact angles of water and n-hexadecane that are larger than 150° (Figure S6, Supporting Information). In the preparation, we use pre-prepared nanofilaments as the substitute of nanoparticles in spray-coating. The NF dispersions for spray-coating were prepared when the air humidity changed from 20% to 40% (Figure S7, Supporting Information). At such humidity region, the superamphiphobic NFSS surface is easy to be reproduced. For comparison, the same process was also used to spray-coat SiO_2 particles on the stretchable substrate. After fluorination, the surface was only superhydrophobic, while the receding contact angle of n-hexadecane on such a surface is almost 0° (Figure S6, Supporting Information). Thus, spray-coating NFs rather than nanoparticles leads to a better liquid repellency and it means our method has obviously reduced the complexity of preparation of the stretchable superamphiphobic surface.

Drop impact experiments show the mechanical stability of the surface against droplet impalement in the relaxed state. Both water (Weber number We = 7.1; $We = \rho U_0^2 R/\gamma$, where ρ is the density, U_0 is the impacting velocity, R is the radius of the drop and γ is the liquid–air surface tension) and n-hexadecane (We = 11.1) bounce from the relaxed NFSS surface ($\varepsilon = 0\%$) with no retention (Figure 1e,f). The porous microstructure increases the impalement pressure of the surface and prevents the three-phase contact line from moving downward on the structure. Moreover, given a stable superamphiphobicity, both water and n-hexadecane sessile drops maintain spherical shapes on the stretched NFSS surface, even at a strain $\varepsilon \approx 200\%$ (Figure 1g).

The NFSS surface in the stretched state exhibits stable superliquid-repellent performance to both water and n-hexadecane (**Figure 2**a). To avoid the effects of the inhomogeneous tensile strength on the stretched NFSS surface,[23] the advancing and receding contact angles (Θ_{ACA} and Θ_{RCA}) and the roll-off angles ($\alpha_{roll\text{-}off}$) of liquids were all measured in the middle area. The surface maintains high receding contact angles ($\Theta_{RCA} > 150°$) for both water and n-hexadecane and low roll-off angles (10 μL water, $\alpha_{roll\text{-}off} \leq 1.2°$ and 10 μL hexadecane, $\alpha_{roll\text{-}off} \leq 3.3°$) up to $\varepsilon \leq 225\%$. At $\varepsilon = 250\%$, the NFSS surface was still superhydrophobic. However, both Θ_{ACA} and Θ_{RCA} of n-hexadecane are lower than 150° (Figure S8, Supporting Information). Nevertheless, 10 μL n-hexadecane drops still rolled off

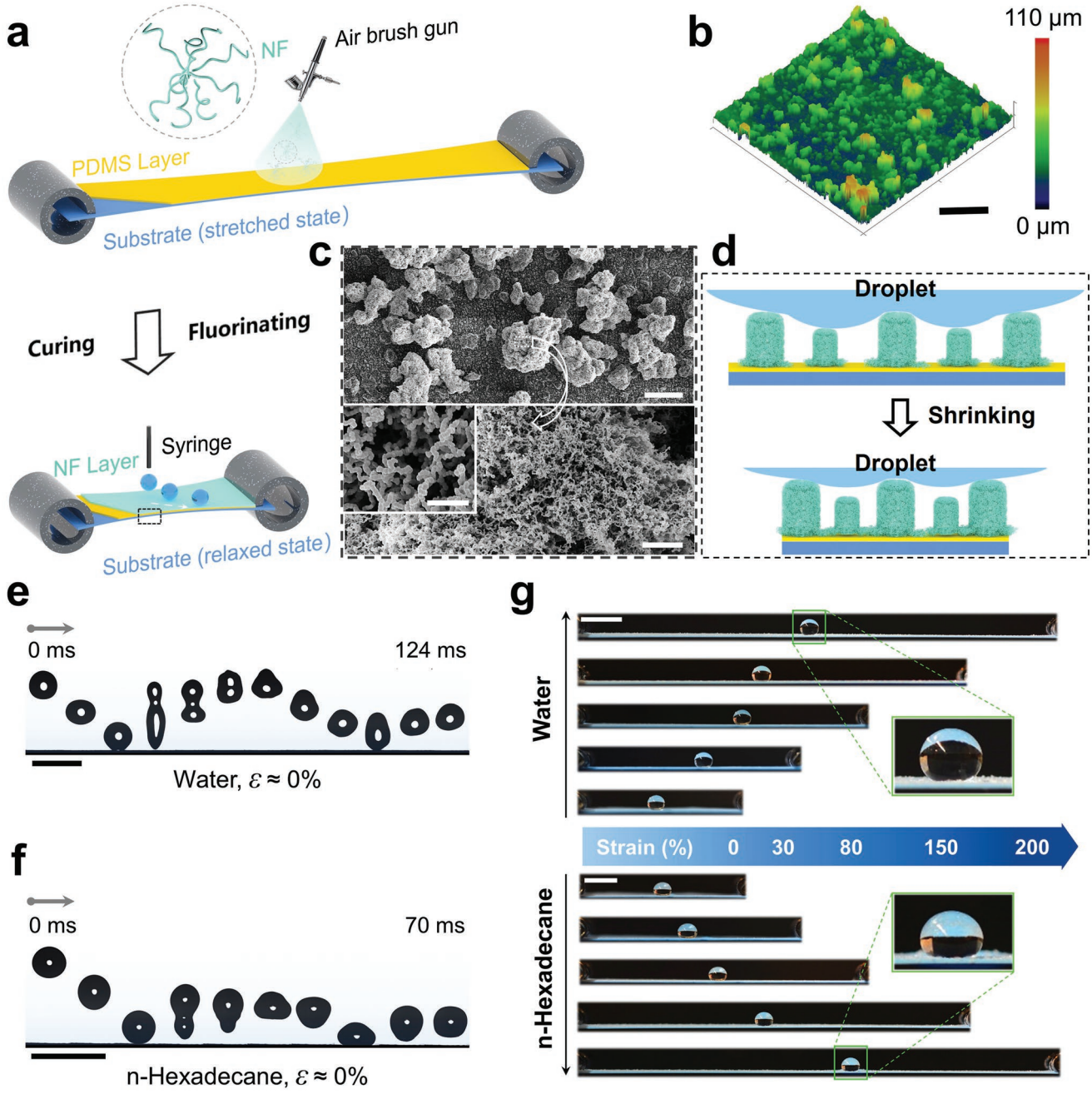

Figure 1. The nanofilament-structured and stretchable superamphiphobic surface. a) Schematic of the fabrication process of the nanofilament-structured and stretchable superamphiphobic (NFSS) surface. b) 3D images taken by Nanofocus μsurf 3D confocal surface measurement system of the NFSS surface at $\varepsilon \approx 0\%$. Scale bar: 200 μm. c) Scanning electronic microscopy (SEM) images of the NFSS surface at $\varepsilon \approx 0\%$. Scale bar: 50 μm (top), 2 μm (bottom), and 500 nm (inset). d) Schematic to illustrate the changing of microstructures on the NFSS surface after releasing the surface. e) Image series show the impact and bouncing of one 6 μL water drop on the NFSS surface ($\varepsilon \approx 0\%$). Drop release height: 2 cm, scale bar: 5 mm. f) Image series show the impact and bouncing of one 3 μL n-hexadecane drop on the NFSS surface ($\varepsilon \approx 0\%$). Drop release height: 2 cm, scale bar: 5 mm. g) Optical images of spherical shapes of 6 μL water and n-hexadecane drops on the NFSS surface under various strains ranging from 0 to 200%. Scale bar: 5 mm.

the surface at a low tilting angle of 3.4° ± 0.3° when $\varepsilon \approx 250\%$. In contrast, if the NFSS surface is fabricated without pre-stretching, the surface loses its superamphiphobicity at $\varepsilon \geq 50\%$ (Figure S9, Supporting Information).

The accessibility of the surface superamphiphobicity during stretching is determined by the liquid entry or impalement pressure P_{LEP}.[24] P_{LEP} represents the pressure required to force the transition from the nonwetting Cassie state to the fully wetted Wenzel state. For a particular liquid, the microstructure size and spacing usually affect the value of P_{LEP}.[25] Here, we use the average distance between adjacent edges of two NF clusters to illustrate the average structure spacing. When the NFSS surface is stretched, the separation and rearrangement of the structure allow slight changes in both the spacing and the

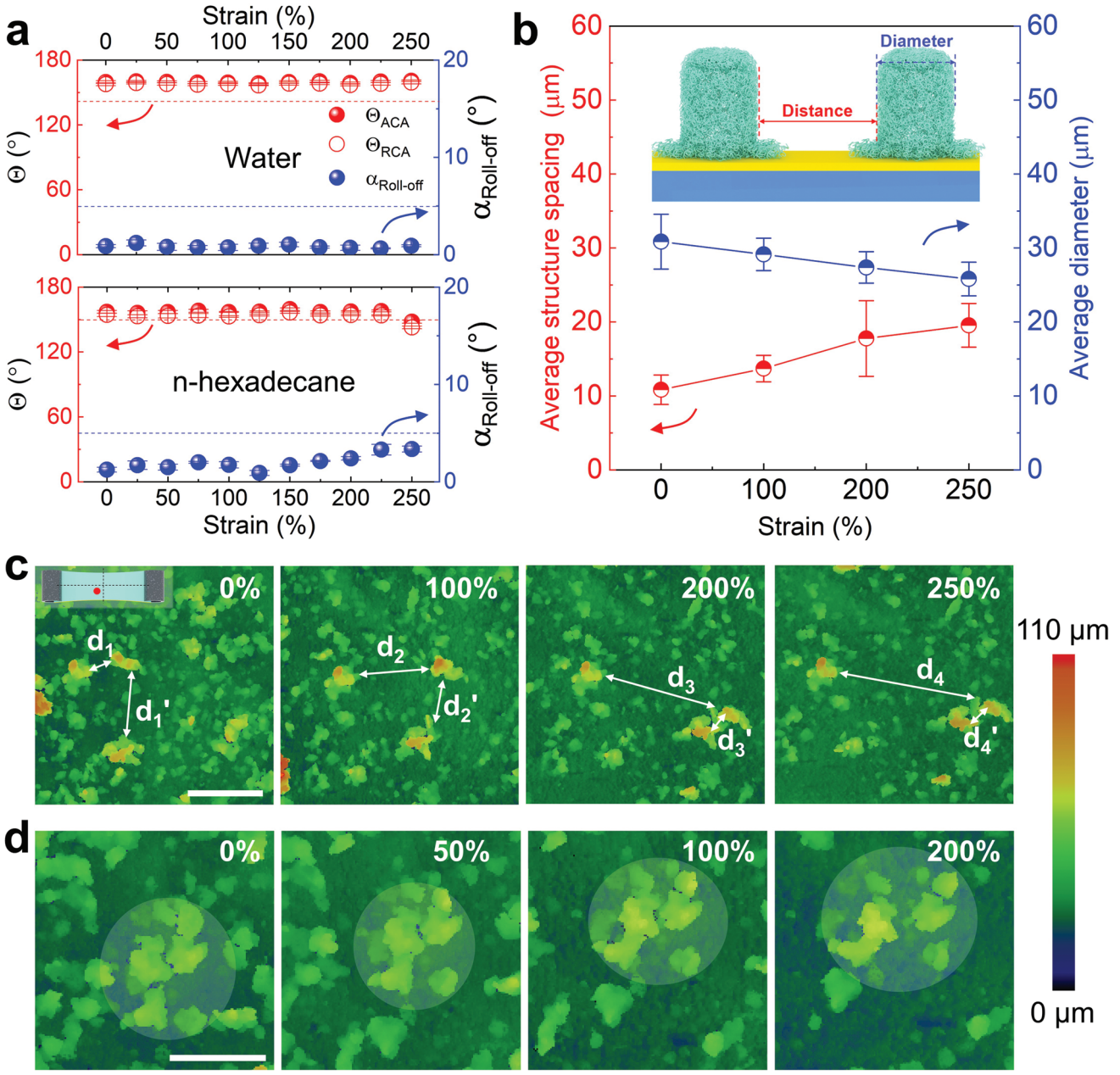

Figure 2. Superamphiphobicity of the stretched NFSS surface. a) Advancing and receding contact angles (Θ_{ACA} and Θ_{RCA}) and roll-off angles ($\alpha_{roll\text{-}off}$) of water and n-hexadecane on the NFSS surface with different tensile strains. Drop volume used in roll-off angle measurement was 10 μL. b) Evolution of the average structure spacing (distance between two NF clusters) and the average cluster size (diameter of the NF cluster) with the change of the surface tensile strain. c) Images using a Nanofocus μsurf 3D confocal surface measurement system illustrate variation of the morphologies when the NFSS surface was stretched. Strain: 0%, 100%, 200%, and 250%. The inset illustrates the measurement position (red dot) of the NFSS surface. Scale bar: 200 μm. d) Images show a rearranging process of the compacted microstructures after stretching from 0% to 200%. Scale bar: 200 μm. The color bar to the right of (c) and (d) illustrates the measured height.

cluster size (Figure 2b). As a result, the NFSS surface exhibits a quite stable superamphiphobicity resisting stretching because of the slightly changed liquid entry pressure.

A Nanofocus μsurf 3D confocal surface measurement system (Nanofocus AG, Oberhausen, Germany) was used to monitor the topography of the NFSS surface in situ during the stretching process (Figure 2c,d). The result shows that when the surface was stretched in one direction, and the distances of NF clusters along the stretching direction increased (e.g., $d_1 < d_2 < d_3 < d_4$) with the strain increasing from 0% to 250%, while the distance of the clusters vertical to the stretching direction decreased (e.g., $d_1' > d_2' > d_3' > d_4'$) (Figure 2c). Some compacted structures split and rearrange at high strain (Figure 2d), and thereby the average diameter of the NF cluster decreases with the increasing tensile strain. In our view, the splitting of the structures into smaller clusters and the

rearrangement of them during the stretching process prevent breakup of the NF coating layer and the formation of big cracks to ensure that thus the surface maintains a stable superamphiphobicity. Finally, the surface loses its superamphiphobicity due to the low coverage of the NF cluster at a high tensile strain, in our case at $\varepsilon \approx 250\%$.

A continuous and alternating stretch–release test was conducted to illustrate the mechanical durability of the NFSS surface (Figure S10a, Supporting Information). The surface was repeatedly stretched along one direction with a speed of 0.4 cm s^{-1} to $\varepsilon \approx 100\%$ and then released to $\varepsilon \approx 0\%$ with the same speed again. During stretch–release cycles, both water and n-hexadecane rebounded and rolled off the surface (Figure S10b,c, Movie S1, Supporting Information). After 1000 cycles, both water and n-hexadecane still have a high receding contact angle ($\Theta_{RCA} > 150°$) and low contact angle hysteresis (**Figure 3**a). Here, Θ_{ACA} and Θ_{RCA} were measured when the tensile strain of the NFSS surface was 0% and

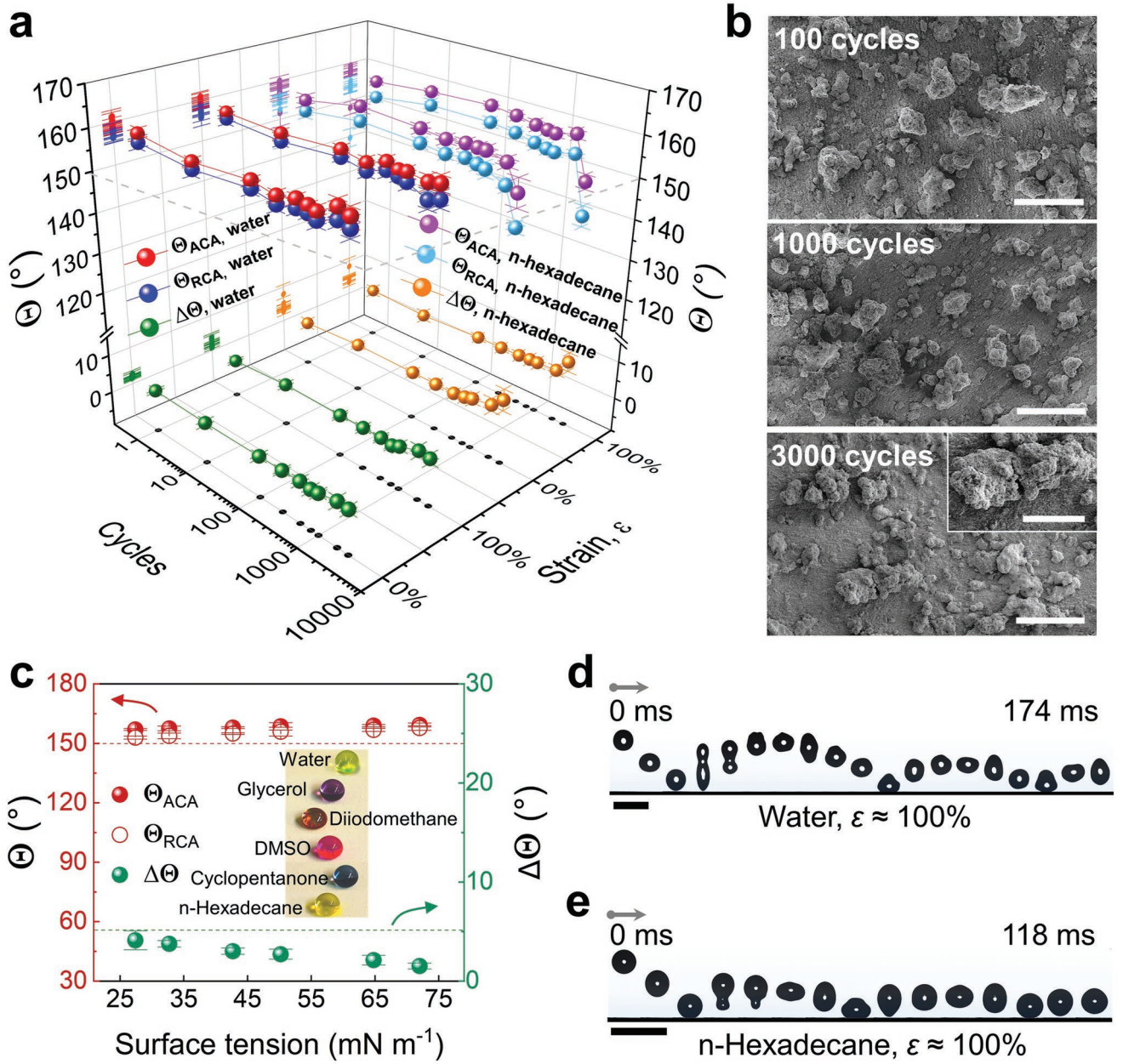

Figure 3. Durability of the NFSS surface after repeated stretching. a) Θ_{ACA}, Θ_{RCA}, and $\Delta\Theta$ of water and n-hexadecane on the NFSS surface after different stretch–release cycles. The contact angles were measured at $\varepsilon \approx 0\%$ and $\varepsilon \approx 100\%$, respectively. b) SEM images of the NFSS surface after 100, 1000, and 3000 stretch–release cycles. Scale bar: 100 and 50 µm (inset). c) Θ_{ACA}, Θ_{RCA}, and $\Delta\Theta$ of various liquids on the stretched NFSS surface ($\varepsilon \approx 100\%$) after 1000 cycles of test. Inset shows the image of sessile drops (10 µL) of corresponding liquids on the stretched NFSS surface. d) Image series showing the impact and bouncing of a 6 µL water drop on the surface. Release height: 2 cm; scale bar: 5 mm; $\varepsilon \approx 100\%$. e) Image series of the impact and bouncing of a 3 µL n-hexadecane drop on the surface. Drop release height: 2 cm; scale bar: 5 mm; $\varepsilon \approx 100\%$.

100%, respectively. According to the SEM images (in random positions), the morphologies of the surface after 100 and 1000 stretch–release cycles seem not to change qualitatively (Figure 3b). After 1000 cycles, the NFSS surface is still superamphiphobic to a wide range of liquids even if it is stretched to 100% (Figure 3c). Besides water (γ = 72.2 mN m^{-1}) and hexadecane (γ = 27.4 mN m^{-1}), other liquids including glycerol (γ = 64.8 mN m^{-1}), diiodomethane (γ = 50.2 mN m^{-1}), dimethyl sulfoxide (DMSO, γ= 42.7 mN m^{-1}) and cyclopentanol (γ= 32.7 mN m^{-1}) all maintain spherical shapes on the surface with high receding contact angles ($\Theta_{RCA} > 150°$) and low contact angle hysteresis ($\Delta\Theta = \Theta_{ACA} - \Theta_{RCA} < 5°$). The surface can still withstand liquid drop impact after 1000 cycles of stretch–release test (Figure 3d,e). When ε was about 100%, both water (We = 7.1) and n-hexadecane (We = 11.1) drops rebounded at least three times. No retention caused by the impact was observed on the surfaces. This enduring repellency is likely due to the high coverage of the re-entrant structures. Although the surface is still superhydrophobic after 3000 stretch–release cycles, contact angle measurements show that the NFSS surface starts to lose the superoleophobicity. This is reflected by the receding contact angle of hexadecane on both relaxed and stretched surfaces being lower than 150° (Figure 3a). The rearrangement seems to be irreversible after 3000 cycles as big cracks happen on the cluster because of a failing regrouping process (Figure 3b, 3000 cycles inset).

Besides the stretch durability, we further characterized the mechanical stability of the NFSS surface against sand abrasion (Figure S11, Supporting Information). After testing for more than 5 min, the appearance of the coating changed little. Drops of water (30 µL) and n-hexadecane (20 µL) still easily slide off the surface with tilting angle of 45°. According to the contact angle measurements, the superamphiphobicity of the surface does not change with receding contact angles being lager than 150° when the surface is in both relaxed and stretched states after the test. A sandpaper abrasion test was further conducted, in which NFSS loaded with a weight of 30 g were placed face down on a sandpaper (Starcke P1000) (Figure S12, Supporting Information). The abrasion area was about 4.2 cm^2 and thereby the loaded pressure during the test was around 0.72 kPa which is within the range of the pressure values previously reported.[26] We define a movement of 10 cm of the surface along the ruler as one abrasion cycle. After 10 cycles of abrasion, the surface still maintains its superhydrophobicity, but has lost its superoleophobicity. The receding contact angle of water remained around 155°, while the contact angle of n-hexadecane decreased from 153° to 140°. From the SEM images, we observed that after 10 cycles of abrasion, the NFSS morphology was destroyed into pieces and no obvious compact cluster could be observed anymore. Nevertheless, the remained structures fixed by the binding layer were still superhydrophobic. The NFSS surface with a good mechanical stability against both deformation and abrasion has potential real applications including artificial skin, flexible electronics and dressings.

By taking advantage of the repellency to low-surface-tension liquids and the stretchability of the NFSS surface, we developed a setup that can help achieve repetitive drops coalesce in a controlled way (**Figure 4**a). Two drops were placed side by side onto a stretched NFSS surface. When the surface was gradually released, the decreasing distance between the drops finally led to the drops coming into contact and coalescing. Two water drops (15 µL) or two n-hexadecane drops (10 µL) can be placed on a stretched NFSS surface with ε = 100% (Figure S13, Movie S2 and S3, Supporting Information). Releasing the surface, drops coalesced and formed a merged spherical drop. After removing the merged drop, the drop coalescing process can repetitive occur if two new drops are placed on the NFSS surface which is stretched again. Since even small water drops have a low roll-off angle ($\alpha_{roll\text{-}off} \leq 1°$), placing and keeping them on the surface is difficult. Therefore, poly(vinyl alcohol) hydrophilic dots (diameter: 0.5 mm) were introduced on the stretchable surface to fix the water drops (Figure S14a, Supporting Information). For hexadecane drops with their higher roll-off angle ($\alpha_{roll\text{-}off} \approx 3°$), no hydrophilic dots were necessary (Figure S14b, Supporting Information).

A programmable coalescence of a sequence of drops was then orchestrated. We define programmable manipulation here as the coordinated approach to control the movement and the coalescing sequence of droplets. As an example, a trapezoidal arrangement of water drops was controlled to coalesce on the NFSS surface ($\varepsilon \approx$ 100%) (Figure 4b). When the surface was gradually released, the two middle drops coalesce. Subsequently, coalescence with the drops on the left and right hand side respectively of the merged drop occurs (Movie S4, Supporting Information). This is because the distance between the two drops in the middle was smaller than the distance between the drop on the outside and one of the middle drops. Furthermore, four n-hexadecane drops were linearly arranged on a stretched NFSS surface ($\varepsilon \approx$ 100%) in the stretching direction (Figure 4c). When the surface was released, these drops merged in a certain order from left to right (Movie S5, Supporting Information). This programmable drop manipulation method provides a possible one-by-one reaction process which could be described as A+B → A+B+C → A+B+C+D. It is noted that the NFSS surface based liquid manipulation system can be reusable due to its low adhesion to liquids.

The programmable coalescence of drops on this stretchable superamphiphobic surface was not limited to miscible liquids. One n-hexadecane and two water drops were placed on a stretched NFSS surface (Figure 4d) at appropriate distances. After coalescence, a merged drop with a dumbbell-like shape formed with an apparent interface between these two different drops. This led us to synthesize asymmetric or Janus particles by manipulating drop coalescence with two immiscible liquids. As an example, we synthesized asymmetric hydrogels with two reactive liquid drops (Figure 4e and Figure S15, Supporting Information). Drops of sodium alginate aqueous solution (0.05 wt%) and iron chloride ($FeCl_3$) aqueous solution (1.00 wt%) were placed on the NFSS surface. The reaction of sodium alginate and $FeCl_3$ started when the drops came into contact, after which the iron ions diffused rapidly in the alginate drop (Figure S15a, Supporting Information). As a result, the alginate drop became a hydrogel in a short time, while the $FeCl_3$ drops remained liquid. After removing the $FeCl_3$ drops, hydrogels with different shapes were prepared. We controlled the coalescence of two, three, and four drops. Depending on the numbers and relative position of the drops, hemispherical, cylinder-like, and triangular prism-like hydrogels have been

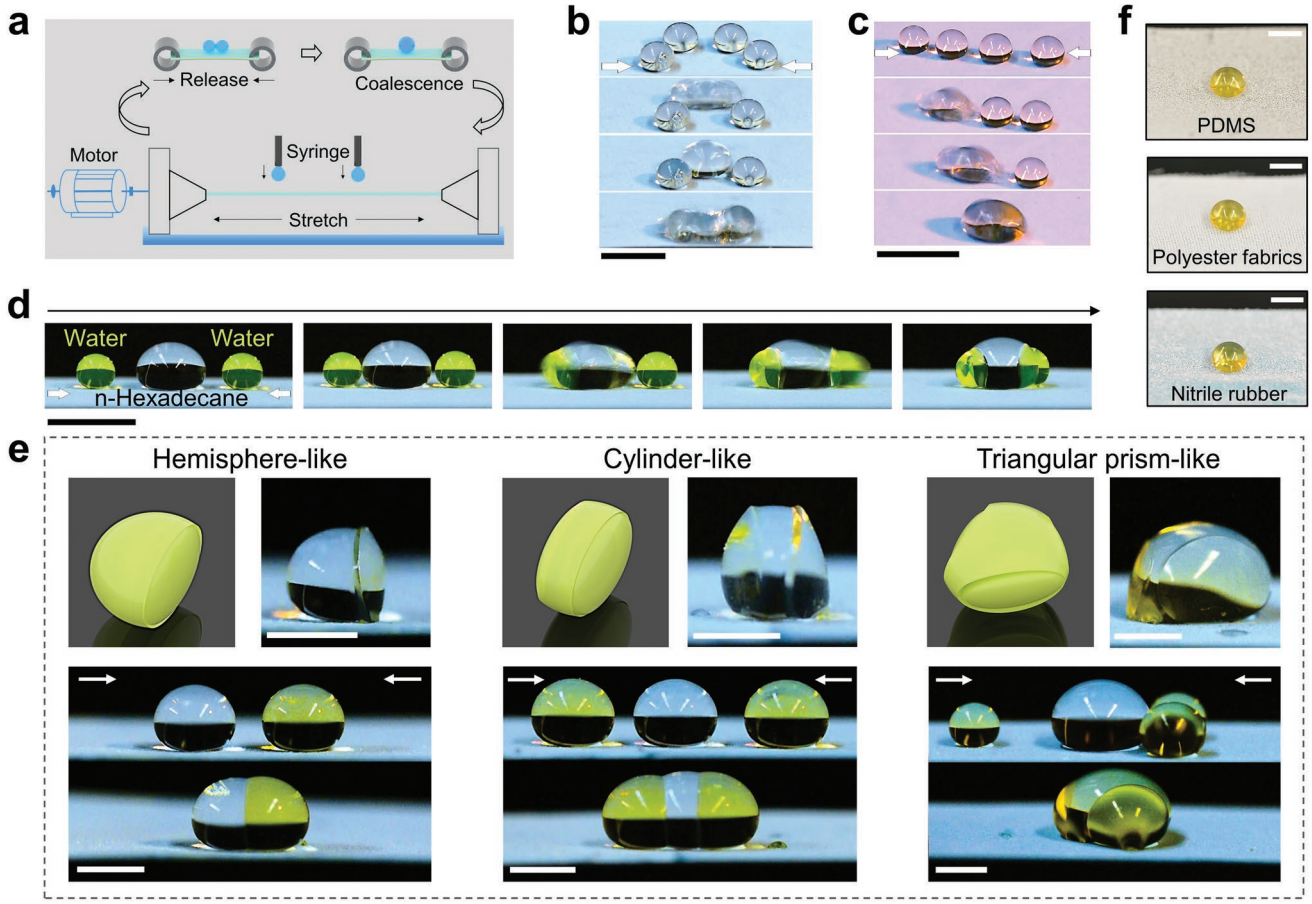

Figure 4. Programmable manipulation of drop coalescences and synthesis of asymmetric hydrogels. a) Schematic to show the setup with a controllable motor to manipulate drop coalescences repetitively. Drops on the surface coalesce via controlled release of the stretched NFSS surface. b) Programmable coalescence of four water drops (15 µL) with a trapezoidal arrangement. Scale bar: 5 mm. c) Programmable coalescence of four n-hexadecane drops (10 µL) with a linear arrangement. Scale bar: 5 mm. d) Coalescence of one n-hexadecane drop (colorless) and two water drops (light green) on the NFSS surface. Scale bar: 5 mm. e) Fabrication of asymmetric hydrogels with specific shapes. One alginate sodium aqueous solution drop (colorless) and different numbers (from left to right: 1, 2, and 3) of $FeCl_3$ aqueous solution drops (yellow) are used in the hydrogel fabrication process. The top schemes and images present three gels with distinct shapes (from left to right): hemispherical, cylinder-like, and triangular prism-like. The lower images show the coalescence of the drops. Volumes of the alginate drops (from left to right): 20, 20, and 30 µL. Volumes of the $FeCl_3$ drops (from left to right): 20, 20, and 15 µL. Scale bar: 2.5 mm. f) Images show spherical n-hexadecane drop (10 µL) on three different flexible substrates spray-coated with silicone nanofilaments. From top to bottom the substrates are PDMS, PE fabrics, and nitrile rubber. Scale bar: 2 mm.

fabricated. By adjusting the volume ratios of the sodium alginate drop to the $FeCl_3$ drop, it is possible to make more kinds of variably shaped hydrogels (Figure S15b,c, Supporting Information).

We further illustrate the fabrication of other three stretchable superamphiphobic surfaces with substrates of cross-linked poly(dimethylsiloxane) (PDMS), polyester (PE) fabrics, and nitrile rubber, in turn. All these surfaces were pre-stretched to their maximum strains during the coating process. Hexadecane drops show high static contact angles ($\Theta > 150°$), low contact angle hysteresis ($\Delta\Theta < 5°$) and roll-off angles ($\alpha_{\text{roll-off}} < 5°$) on all these surfaces (Figure 4f and Figure S16, Supporting Information).

3. Conclusion

We have fabricated a stretchable superamphiphobic surface by spray-coating nanofilaments on a pre-stretched substrate. After drying, annealing, and fluorination, the surfaces were able to withstand at least one thousand stretch–release cycles between $\varepsilon \approx 0\%$ and $\varepsilon \approx 100\%$ with no loss of superamphiphobicity. By using the stretching property, we were able to control the coalescence of miscible and immiscible liquid drops on the surface. We demonstrated that stretchable superamphiphobic surfaces can be applied to let drops react in a programmable manner. This outcome offers us the potential of using stretchable superamphiphobic surfaces to fabricate low-cost, reusable, and programmable droplet-based microfluidic systems which could help to study the reactions or interactions of multidrops.

4. Experimental Section

Preparation of Silicone Nanofilament Dispersion: 1.6 mL of trichloromethylsilane (TCMS, 99.0%, Merck Chemicals GmbH, Germany) was dissolved in 400 mL of toluene (water concentration is

about 150 ppm). The vessel with a narrow mouth was left open to the air (at about 30% relative humidity). Under stirring for more than 12 h, silicone nanofilaments were formed in toluene. The final dispersion was diluted to 0.1 wt% and sonicated for about 30 min.

Fabrication of a Nanofilament-Structured and Stretchable Superamphiphobic (NFSS) Surface: A commercial *cis*-1,4-polyisoprene tape (length: 3.8 cm, width: 1.8 cm, thickness: 0.5 mm, Melloc Handelsgesellschaft and Agentur GmbH, Germany) was used as the substrate. The tape was then stretched to a tensile strain of 200%. After treatment with oxygen plasma (Femto low-pressure plasma system, Diener electronic GmbH, Germany. Treating time is 5 min, the pressure is 0.4 mbar and the power is 200 W, 100%), the stretched substrate was spray-coated with a layer of PDMS oligomers (the ratio of monomer to curing agent is 10:1, Sylgard184, Dow Europe GmbH, Germany) by using a spray gun with a nozzle diameter of 0.2 mm at a spraying pressure of 27 kPa. The sprayed PDMS solution was prepared by dissolving 1.0 g of monomer and 0.1 g curing agent in 20 mL of n-hexane. Subsequently, the nanofilament dispersion was spray-coated onto the substrate by using the same spray gun and spraying pressure. Afterward, the surface held under tension was heated at 80 °C to cure the PDMS layer for 2 h. Then, the surface was cooled to room temperature and treated with oxygen plasma. The surface was further fluorinated with 5 µL trichloro(1H,1H,2H,2H-heptadecafluorodecyl)silane (Alfa Aesar, 96%) by chemical vapor deposition in a vacuum desiccator (Pyrex Labware borosilicate vaccum desiccator, Fisher Scientific GmbH. The desiccator was evacuated to less than 100 mbar.) for 12 h. Finally, the tensile force was removed and the tape was allowed to relax.

Morphology Characterization: The samples were coated with a thin layer of platinum (7 nm) by a sputtering process, and then the samples were imaged by scanning electron microscopy (SEM, Hitachi SU8000). The in situ images of the morphologies of this surface with different tensile strains were characterized by a Nanofocus μsurf 3D confocal surface measurement system (Nanofocus AG, Oberhausen, Germany). The light of Nanofocus confocal system was focused through a multipinhole disk (MPD) and the objective lens onto the sample surface. The reflected light was detected by the camera to obtain confocal images. Each confocal image was a horizontal and nanometer-range-resolution slice through the topography of the sample. Capturing the images at different focal heights gave hundreds of confocal images which could be reconstructed an exact 3D height image of the sample by Gwyddion.[27] For calculating the average structure spacing and average diameter, the microstructures were marked by circles with comparable size in the Nanofocus confocal images. The Feret diameter (D) of each cluster was obtained by measuring the diameter of the circles. The average structure spacing was measured according to the distance between the edges of the circles.

Wetting Properties: Advancing and receding contact angles as well as the roll-off angles of various liquids on the surfaces were measured by DataPhysics OCA 35 goniometer (DataPhysics Instruments). Each data point was the average of at least three individual measurements on the middle area of the surfaces. Impinging dynamics of water and n-hexadecane drops were recorded by a Photron Fastcam Mini UX100 high-speed camera (4000 fps) with a 2× lens.

Test of the Stretching Robustness: Two sides of a rectangular NFSS surface (length: 4.2 cm, width: 1.8 cm, thickness: 0.5 mm) were fixed and then moved by an electric motor in one direction. Alternatively control of the strain of the surface to be 100% and 0% by the motor. Water or n-hexadecane were dropped on the surface once during each stretch–release cycle, so that it could be checked if the surface still has a good superamphiphobicity. The dynamics were recorded by a Nikon D7100 digital camera (60 fps). After a certain number of stretch–release cycles, the contact angles of water and n-hexadecane were measured on the surface with strain of 0% and 100%, respectively.

Manipulation of Drop Coalescence: A rectangular NFSS surface (length: 4.2 cm, width: 1.8 cm, thickness: 0.5 mm) was fixed at two sides in the motor-controlled stretching setup. Drops were placed on a stretched NFSS surface (typical strain ≈ 100%) with specific distances. Different drops with different components were used. When the surface was released, drops coalesce in turn. The process was recorded by a Nikon D7100 digital camera (60 fps). For the synthesis of asymmetric hydrogel, drops of sodium alginate aqueous solution (0.05 wt%) and iron chloride ($FeCl_3$) aqueous solution (1.00 wt%) were placed on the NFSS surface.

Supporting Information

Supporting Information is available from the Wiley Online Library or from the author.

Acknowledgements

This project received funding from the European Research Council (ERC) under the European Union's Horizon 2020 research and innovation program (grant agreement No 883631, DYNAMO). The authors are also grateful for the financial support from the European Union's Horizon 2020 research and innovation program under grant agreement No 801229. X.Z. is sponsored by the China Scholarship Council (CSC). Helma Burg and Andreas Best are acknowledged for the technical support.

Conflict of Interest

The authors declare no conflict of interest.

Author Contributions

X.Z. and J.L. designed and performed research. X.Z., J.L., W.L., W.S., and H.-J.B. contributed new reagents/analytic tools. X.Z. and J.L. analyzed data. X.Z., J.L., W.L., W.S., and H.-J.B. wrote the paper. All authors have approved the final version of this manuscript.

Data Availability Statement

The data that support the findings of this study are available from the corresponding author upon reasonable request.

Keywords

deformation resistance, liquid manipulation, stretchable surfaces, superamphiphobicity, wetting

Received: October 2, 2021
Revised: December 21, 2021
Published online: January 31, 2022

[1] a) S. Wu, Y. Du, Y. Alsaid, D. Wu, M. Hua, Y. Yan, B. Yao, Y. Ma, X. Zhu, X. He, *Proc. Natl. Acad. Sci. USA* **2020**, *117*, 11240; b) W. S. Y. Wong, T. P. Corrales, A. Naga, P. Baumli, A. Kaltbeitzel, M. Kappl, P. Papadopoulos, D. Vollmer, H.-J. Butt, *ACS Nano* **2020**, *14*, 3836.

[2] a) G. Luo, L. Wen, K. Yang, X. Li, S. Xu, P. Pi, X. Wen, *Chem. Eng. Sci.* **2020**, *383*, 123125; b) F. Geyer, M. D'Acunzi, C.-Y. Yang, M. Müller, P. Baumli, A. Kaltbeitzel, V. Mailänder, N. Encinas, D. Vollmer, H.-J. Butt, *Adv. Mater.* **2019**, *31*, 1801324.

[3] a) S. Masoud Emarati, M. Mozammel, *Chem. Eng. Sci.* **2020**, *387*, 124046; b) N. Valipour Motlagh, F. C. Birjandi, J. Sargolzaei, N. Shahtahmassebi, *Appl. Surf. Sci.* **2013**, *283*, 636.

[4] a) H. Han, J. S. Lee, H. Kim, S. Shin, J. Lee, J. Kim, X. Hou, S.-W. Cho, J. Seo, T. Lee, *ACS Nano* **2018**, *12*, 932; b) Z. Cheng, H. Liu, H. Lai, Y. Du, K. Fu, C. Li, J. Yu, N. Zhang, K. Sun, *ACS Appl. Mater. Interfaces* **2015**, *7*, 20410.

[5] P. Papadopoulos, L. Mammen, X. Deng, D. Vollmer, H. J. Butt, *Proc. Natl. Acad. Sci. USA* **2013**, *110*, 3254.

[6] a) A. Tuteja, W. Choi, M. Ma, J. M. Mabry, S. A. Mazzella, G. C. Rutledge, G. H. McKinley, R. E. Cohen, *Science* **2007**, *318*, 1618; b) E. M. Domingues, S. Arunachalam, J. Nauruzbayeva, H. Mishra, *Nat. Commun.* **2018**, *9*, 3606; c) J. Zhang, S. Seeger, *Angew. Chem., Int. Ed.* **2011**, *50*, 6652; d) X. Deng, L. Mammen, H.-J. Butt, D. Vollmer, *Science* **2012**, *335*, 67.

[7] a) D. Wang, Q. Sun, M. J. Hokkanen, C. Zhang, F.-Y. Lin, Q. Liu, S.-P. Zhu, T. Zhou, Q. Chang, B. He, Q. Zhou, L. Chen, Z. Wang, R. H. A. Ras, X. Deng, *Nature* **2020**, *582*, 55; b) H. Bellanger, T. Darmanin, E. Taffin de Givenchy, F. Guittard, *Chem. Rev.* **2014**, *114*, 2694; c) Z. Chu, S. Seeger, *Chem. Soc. Rev.* **2014**, *43*, 2784; d) J. Yong, F. Chen, Q. Yang, J. Huo, X. Hou, *Chem. Soc. Rev.* **2017**, *46*, 4168.

[8] a) B. Choi, J. Lee, H. Han, J. Woo, K. Park, J. Seo, T. Lee, *ACS Appl. Mater. Interfaces* **2018**, *10*, 36094; b) L. Li, Y. Bai, L. Li, S. Wang, T. Zhang, *Adv. Mater.* **2017**, *29*, 1702517.

[9] a) J. N. Wang, Y. Q. Liu, Y. L. Zhang, J. Feng, H. Wang, Y. H. Yu, H. B. Sun, *Adv. Funct. Mater.* **2018**, *28*, 1800625; b) R. Shimizu, Y. Nonomura, *J. Oleo Sci.* **2018**, *67*, 47.

[10] a) L. Xiong, L. L. Kendrick, H. Heusser, J. C. Webb, B. J. Sparks, J. T. Goetz, W. Guo, C. M. Stafford, M. D. Blanton, S. Nazarenko, D. L. Patton, *ACS Appl. Mater. Interfaces* **2014**, *6*, 10763; b) H. Zou, S. Lin, Y. Tu, F. Li, J. Hu, G. Liu, S. Hu, G. Yang, Z. Yu, *Adv. Mater. Interfaces* **2016**, *3*, 1500693.

[11] a) S. Y. W. William, L. Guanyu, T. Antonio, *Small* **2017**, *13*, 1603688; b) J.-Y. Huang, Y.-K. Lai, F. Pan, L. Yang, H. Wang, K.-Q. Zhang, H. Fuchs, L.-F. Chi, *Small* **2014**, *10*, 4865.

[12] a) S. Pan, R. Guo, M. Björnmalm, J. J. Richardson, L. Li, C. Peng, N. Bertleff-Zieschang, W. Xu, J. Jiang, F. Caruso, *Nat. Mater.* **2018**, *17*, 1040; b) W. Li, Y. Zong, Q. Liu, Y. Sun, Z. Li, H. Wang, Z. Li, *Prog. Org. Coat.* **2020**, *147*, 105776; c) W. Hujun, Z. Zhihui, W. Zuankai, L. Yunhong, C. Zhenquan, Z. Jie, L. Xiujuan, R. Luquan, *ACS Appl. Mater. Interfaces* **2019**, *11*, 28478; d) A. Grigoryev, I. Tokarev, K. G. Kornev, I. Luzinov, S. Minko, *J. Am. Chem. Soc.* **2012**, *134*, 12916; e) W. Wang, J. Salazar, H. Vahabi, A. Joshi-Imre, W. E. Voit, A. K. Kota, *Adv. Mater.* **2017**, *29*, 1700295.

[13] W. S. Y. Wong, G. Y. Liu, N. Nasiri, C. L. Hao, Z. K. Wang, A. Tricoli, *ACS Nano* **2017**, *11*, 587.

[14] a) A. Y. Fadeev, T. J. McCarthy, *Langmuir* **2000**, *16*, 7268; b) C. P. Tripp, M. L. Hair, *Langmuir* **1995**, *11*, 149; c) G. E. Maciel, M. J. Sullivan, D. W. Sindorf, *Macromolecules* **1981**, *14*, 1607; d) K. A. Andrianov, T. V. Vasil'eva, N. M. Katashuk, T. V. Snigireva, B. I. D'Yachenko, *Polym. Sci. U.S.S.R* **1976**, *18*, 1457.

[15] S. Liu, X. Zhang, S. Seeger, *ACS Appl. Mater. Interfaces* **2019**, *11*, 44691.

[16] a) W. Tao, L. Chang, J. Lvlv, H. Xia, W. Sheng, *ACS Appl. Mater. Interfaces* **2020**, *12*, 49155; b) S. Dong, B. Li, J. Zhang, A. Wang, *Adv. Mater. Interfaces* **2018**, *5*, 1701520.

[17] a) Z. Li, M. Cao, P. Li, Y. Zhao, H. Bai, Y. Wu, L. Jiang, *Matter* **2019**, *1*, 661; b) Z. Nie, E. Kumacheva, *Nat. Mater.* **2008**, *7*, 277; c) B. Zdyrko, V. Klep, I. Luzinov, *Mater. Matters* **2008**, *3*, 44.

[18] a) J. Genzer, K. Efimenko, *Science* **2000**, *290*, 2130; b) K. Efimenko, M. Rackaitis, E. Manias, A. Vaziri, L. Mahadevan, J. Genzer, *Nat. Mater.* **2005**, *4*, 293.

[19] C. Cao, H. F. Chan, J. Zang, K. W. Leong, X. Zhao, *Adv. Mater.* **2014**, *26*, 1763.

[20] J. Ju, X. Yao, X. Hou, Q. Liu, Y. S. Zhang, A. Khademhosseini, *J. Mater. Chem. A* **2017**, *5*, 16273.

[21] K. Efimenko, J. Finlay, M. E. Callow, J. A. Callow, J. Genzer, *ACS Appl. Mater. Interfaces* **2009**, *1*, 1031.

[22] a) Y. Ma, K.-I. Jang, L. Wang, H. N. Jung, J. W. Kwak, Y. Xue, H. Chen, Y. Yang, D. Shi, X. Feng, J. A. Rogers, Y. Huang, *Adv. Funct. Mater.* **2016**, *26*, 5345; b) V. Tanrattanakul, N. Sungthong, P. Raksa, *Polym. Test.* **2008**, *27*, 794.

[23] J. Genzer, D. A. Fischer, K. Efimenko, *Adv. Mater.* **2003**, *15*, 1545.

[24] A. K. Kota, Y. Li, J. M. Mabry, A. Tuteja, *Adv. Mater.* **2012**, *24*, 5838.

[25] a) A. Tuteja, W. Choi, G. H. McKinley, R. E. Cohen, M. F. Rubner, *MRS Bull.* **2008**, *33*, 752; b) S. S. Chhatre, W. Choi, A. Tuteja, *Langmuir* **2010**, *26*, 4027.

[26] a) H. Cho, D. Kim, C. Lee, W. Hwang, *Curr. Appl. Phys.* **2013**, *13*, 762; b) M. Li, Y. Li, F. Xue, X. Jing, *Appl. Surf. Sci.* **2019**, *480*, 738; c) J. Song, Y. Li, W. Xu, H. Liu, Y. Lu, *J. Colloid Interface Sci.* **2019**, *541*, 86; d) P. Wang, B. Sun, T. Yao, M. Chen, X. Fan, H. Han, L. Li, C. Wang, *Chem. Eng. Sci.* **2017**, *326*, 1066; e) L. Chen, X. Sun, J. Hang, L. Jin, D. Shang, L. Shi, *Adv. Mater. Interfaces* **2016**, *3*, 1500718; f) P. Varshney, S. S. Mohapatra, *Tribol. Int.* **2018**, *123*, 17; g) D. Zhang, L. Li, Y. Wu, B. Zhu, H. Song, *Appl. Surf. Sci.* **2019**, *473*, 493; h) P. Wang, B. Sun, Y. Liang, H. Han, X. Fan, W. Wang, Z. Yang, *J. Mater. Chem. A* **2018**, *6*, 10404; i) A. Davis, S. Surdo, G. Caputo, I. S. Bayer, A. Athanassiou, *ACS Appl. Mater. Interfaces* **2018**, *10*, 2907.

[27] D. Nečas, P. Klapetek, *Open Phys.* **2012**, *10*, 181.